Single-molecule photocurrent at a metal-molecule-semiconductor junction

Andrea Vezzoli[a], Richard J. Brooke[b], Simon J. Higgins[a], Walther Schwarzacher[b*], and Richard J. Nichols[a*]

a) Department of Chemistry, University of Liverpool, Crown Street, Liverpool L69 7ZD, United Kingdom

b) H. H. Wills Physics Laboratory, University of Bristol, Tyndall Avenue, Bristol BS8 1TL, United Kingdom

* Corresponding authors: E-mail: nichols@liv.ac.uk

E-mail: w.schwarzacher@bristol.ac.uk

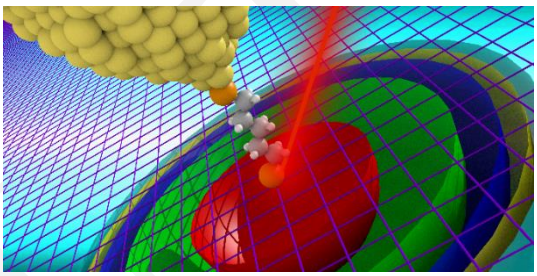

Abstract: We demonstrate here a new concept for a metal-molecule-semiconductor nanodevice employing Au and GaAs contacts that acts as a photodiode. Current-voltage traces for such junctions are recorded using a STM and the "blinking" or "I(t)" method is used to record electrical behaviour at the single-molecule level in the dark and under illumination, with both low and highly doped GaAs samples and with two different types of molecular bridge: non-conjugated pentanedithiol and the more conjugated 1,4-phenylene(dimethanethiol). Junctions with highly doped GaAs show poor rectification in the dark and a low photocurrent while junctions with low doped GaAs show particularly high rectification ratios in the dark (> 10^3 for a 1.5 V bias potential) and a high photocurrent in reverse bias. In low doped GaAs the greater thickness of the depletion layer not only reduces the reverse bias leakage current but also increases the volume that contributes to the photocurrent, an effect amplified by the point contact geometry of the junction. Furthermore, since photo-generated holes tunnel to the metal electrode assisted by the HOMO of the molecular bridge, the choice of the latter has a strong influence on both the steady state and transient metal-molecule-semiconductor photodiode response. The control of junction current via photo-generated charge carriers adds new functionality to single molecule nanodevices.

Keywords: STM, single molecule junctions, gallium arsenide, photodiode.

The use of single molecules (or nanoscale collections thereof) as active electronic components in a device, has developed from a scientific curiosity to an important tool in the study of the fundamental quantum phenomena dominating charge transport at the nanoscale. Since the pioneering studies 15-20 years ago[1–3], noble metals have been the most widely used contact electrode material for single- or few-molecule junctions,[4–6] mostly due to their behavior as simple ohmic resistors, their insensitivity to oxidation and tarnishing, and the availability of a large range of binding groups that give stable metal-molecule bonds.[7–9] However, non-metallic electrodes are also of interest for single-molecule studies[10,11] and semiconducting electrodes[12–18] have the special advantage that both the molecular entity and the electrodes can be used to impart desired functionalities to the final electrode-molecule-electrode junction. For

PREPRINT

example, in a metal-molecule-semiconductor (MMS) junction the semiconducting electrode can impart a rectifying (diode) behavior, because charge carrier depletion at the junction allows a larger charge flow when the device is biased in one direction (forward bias) than the other (reverse bias). MMS diodes demonstrating a current response at the single-molecule level have been recently reported using GaAs[12] and Si[17] contacts. Simple rectifying behavior, however, is not the only effect that arises in a device with asymmetric (metal-semiconductor) electrodes. When the semiconductor is illuminated with electromagnetic radiation of appropriate wavelength, electrons are promoted to the conduction band and holes are generated in the valence band. Band bending at the junction separates the photo-generated carriers, giving rise to a spontaneous photocurrent even when the device is not biased. Here we show that this photoelectric response can be exploited in single-molecule devices, opening a new channel through which they can react to an external stimulus. Not only do we measure the reverse bias photocurrent through a single molecule for the first time but we demonstrate a novel feature of this type of junction, namely that when a reverse bias is applied the photocurrent does not saturate as it would in a planar device. This is important because it enables the device sensitivity to be tuned via both the semiconductor doping density and the choice of molecule.

We recently reported a MMS device based on a Gallium Arsenide (GaAs) semiconducting electrode,[12] and found that the rectification ratio (current in forward bias / current in reverse bias for a bias of fixed magnitude) is strongly influenced by the nature of the organic compound bridging the metal-semiconductor gap. Furthermore, we could detect single-molecule events in such devices. We focused on GaAs as semiconducting electrode because it is straightforward to build densely packed self-assembled monolayers (SAMs) on its unoxidized surface,[19–21] and because it has a high electron mobility. It also has interesting optoelectronic properties arising from its direct bandgap, which result in more efficient photon absorption when compared to indirect bandgap semiconductors such as Si or Ge. These properties make GaAs an excellent candidate for single-molecule devices based on semiconductor technology. Our use of organic molecules to engineer the response of a nano-scale metal-semiconductor junction in the present work is distinct from the use of electromagnetic radiation to switch a single-molecule device between two states with different charge transport behavior[16,22–26] The latter relies on the optical response of the molecule itself via light-induced isomerization of appropriate organic moieties whereas in our device, the photo-response derives from the semiconductor. Hence, in our device, the photocurrent depends on the level of illumination, rather than being an ON-OFF effect, which could be an advantage for photo-sensing applications.

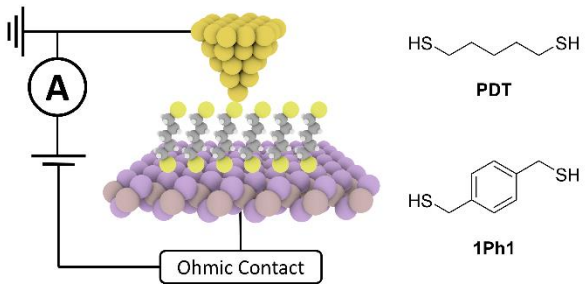

Figure 1: Schematic of the device and structures of the molecular wires used in this study.

PREPRINT

The initial focus of our investigation was the archetypal α,ω-alkanedithiol system. We employed two different n-type <100> GaAs wafers: a highly doped ($GaAs^{HD}$) with 3 x 10^{18} cm^{-3} Si dopant density or a lower doped ($GaAs^{LD}$) with 1.6 x 10^{17} cm^{-3} Si density. We have previously described the technique employed to make and characterize MMS junctions.[12] In brief, a GaAs wafer is cut to a size suitable for the STM sample holder, painted on the back with GaIn eutectic and then annealed for 90 minutes at 400 °C in vacuum (~10^{-5} bar) to provide an ohmic contact. The wafer is then chemically etched and immediately immersed in a degassed ethanol solution containing the desired molecular wire at 1 mM concentration and 5% NH_4OH (to avoid oxide layer regrowth). The sample is then incubated for 24 hours under Ar atmosphere to allow for SAM formation. After this time, the sample is removed from solution, thoroughly rinsed with ethanol, dried under a stream of Ar, and placed on a Au slide with an additional layer of fresh GaIn eutectic painted to provide optimal contact. After mounting the sample in the STM stage, a freshly cut Au tip was driven towards the substrate at a forward bias of -1.5 V (*i. e.* the n-type semiconductor at a negative potential of -1.5 V with respect to the tip) by increasing the setpoint current until single-molecule events[12,17,27] (junction formation / junction breakdown) could be observed in the time-dependent tunneling current traces (schematics of device structure in Figure 1). As discussed previously, under these conditions the STM tip must be in contact with or slightly embedded in the monolayer, thus interacting with a small number of individual molecules.[12] The STM feedback loop was then disabled and we recorded *I / V* characteristics by sweeping the voltage from -1.5 to 1.5 V, at a rate of 3 V / s (bias applied to GaAs substrate). The results are presented in Figure 2. We present data here as the average of 25 separate voltage ramps, because single-molecule bridge formation/rupture can be observed in individual traces (more details in the SI). The procedure was performed in the dark and under illumination, with a HeNe laser focused on the tip-substrate gap at grazing incidence.

A comparison of Figures 2 (a) and (b) shows the critical role of the substrate doping density in determining both the rectification ratio in the absence of light and the photoresponse. 1,5-Pentanedithiol (**PDT**) on $GaAs^{HD}$ (called "PDT:$GaAs^{HD}$") behaves as a leaky Schottky diode (more details in our previous publication[12]), with a low rectification ratio and large dark current at high reverse bias (1.5 V). Illumination produced very little effect on the I / V characteristics. **PDT**:$GaAs^{LD}$, on the other hand, showed minimal dark current at a reverse bias of 1.5 V, with an associated rectification ratio of > 10^3. High rectification ratios were recently reported by Aragones *et al*., for MMS diodes incorporating Si with a low doping density,[17] and attributed to the thicker depletion layer (space charge region) in low doped semiconductors, giving a wider tunneling barrier that prevents electron transport from the metal up to the Schottky breakdown voltage. In the case of **PDT**:$GaAs^{LD}$, we observe appreciable breakdown only at ≈5 V bias (Figure S6).

The true shape of the space charge zone will be more complex,[28] but the essential physics can be understood by assuming a hemispherical geometry. As the bias potential is increased in reverse bias, the radius of the hemispherical space charge region increases (Figure 3

(b)). It is the electric field in the space charge region that sweeps photo-generated holes to the molecular junction while the photo-generated electrons are swept to the semiconductor bulk (Figure 3 (a)). The radius of the laser spot is much larger (a few mm) than the radius of the space charge region. Hence, when the radius of the space charge region increases, the fraction of the illuminated area that contributes charge carriers to the photocurrent also increases, and consequently so does the photocurrent. The absolute photocurrent value (at a given reverse bias) depends on the illumination intensity, but the distinctive increase in photocurrent with increasing reverse bias, characteristic of the molecular contact geometry, is observed independent of illumination intensity. Note that for a planar junction the illuminated area contributing to the photocurrent does not change in this way, so the photocurrent saturates.

The "Hard Contact" $GaAs^{HD}$ junction, which was prepared by crashing the Au STM tip several µm into the semiconductor surface without a molecular layer has a large diameter compared to the molecular junctions and shows a photoelectric response much closer to that expected for a planar junction (see Figure 2 (d)). Solving Poisson's equation for a hemispherical Schottky point-contact[29] gives a space charge region with a radius a factor of 2.7 times smaller for $GaAs^{HD}$, than for $GaAs^{LD}$ (more details in the SI). This is the reason for the much higher photocurrent observed for the **PDT**:$GaAs^{LD}$ junction than **PDT**:$GaAs^{HD}$.

Having established that $GaAs^{LD}$ is a better platform than $GaAs^{HD}$ for the study of photocurrent effects in MMS junctions, we tested the effect of substituting **PDT** with a more conjugated molecular wire. 1,4-Phenylene(dimethanethiol) (**1Ph1**) on $GaAs^{LD}$ also showed high rectification ratios in the dark, though lower than **PDT** (> 10^2), but an even higher photocurrent response upon laser illumination, with values larger than 10 nA at 1.5 V reverse bias.

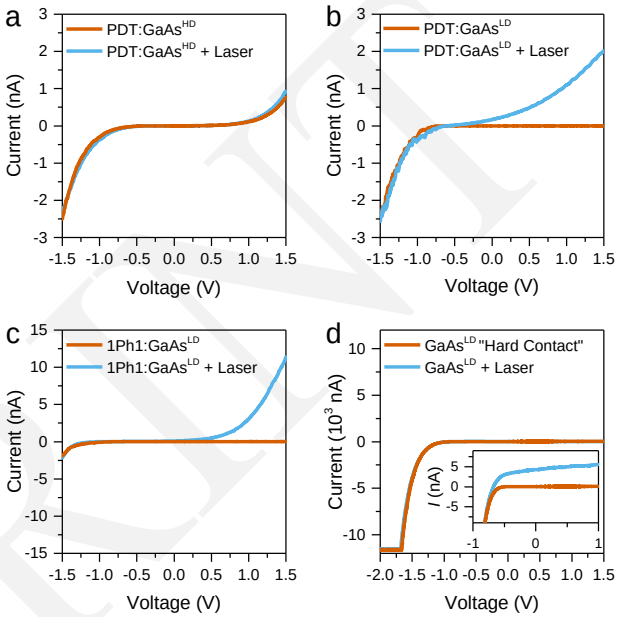

Figure 2: Junction *I / V* characteristics for **PDT** on $GaAs^{HD}$ (a), **PDT** on $GaAs^{LD}$ (b), and **1Ph1** on $GaAs^{LD}$ (c). Data acquired at 2.5 nA setpoint, scanning from forward to reverse bias at 3 V/s. (d) *I / V* characteristics of a "hard contact" between Au and $GaAs^{LD}$ wafers made by crashing the tip several µm into a freshly etched GaAs surface. The inset shows an enlargement of the low-current area between -1 and 1 V. Data acquired scanning from forward to reverse bias at 3 V/s.

Both these results can be explained by the energy alignment between the frontier molecular orbitals and the metal Fermi level. In the case of **PDT**, DFT calculations position the HOMO at an energy about 2.5 eV below the Au Fermi level[30], thus providing a high tunneling barrier. **1Ph1**, due to its increased conjugation, has a lower HOMO-LUMO gap, and the HOMO orbital lies much closer to the Au Fermi level, only about 0.8 eV below its energy.[31] Since the HOMO is closer to the Au Fermi level in the case of **1Ph1** this

PREPRINT

reduces the tunneling barrier height for photo-generated holes and thereby increases the tunneling current. Note that the sulfur-sulfur distances in **1Ph1** and **PDT** are very similar (0.8 nm, calculated using Wavefunction Spartan® software), so that although they have different tunnel barrier heights, they have approximately the same tunneling distance. As discussed in detail in our previous publication,[12] the reason for the higher dark current and therefore lower rectification ration for **1Ph1** is that the energy barrier for electrons tunneling from the metal to the semiconductor conduction band via the LUMO is lower than for **PDT**.

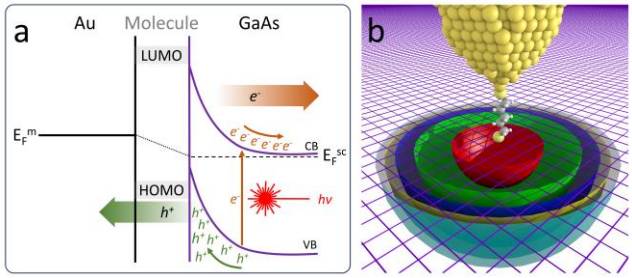

Figure 3: Schematic band diagram for the illuminated MMS junction under reverse bias (a) and simplified depiction of the hemispherical space charge region (b) at different bias values. The ideal space charge region is a red hemisphere at low bias, incrementing through green, blue and yellow to cyan at higher bias. GaAs surface is represented as a purple mesh for clarity.

To characterize the photocurrent response further, with the feedback loop disabled and the tip in shallow contact with the monolayer, we used an optical chopper to alternate the junction between dark and illuminated conditions, and obtain time-dependent reverse bias photocurrent traces (Figure 4). While molecular junctions on $GaAs^{HD}$ show a simple square-wave response with an amplitude of only about 100 pA, the same measurement on $GaAs^{LD}$ results in a sudden increase in current upon illumination, followed by a decay to the steady-state value observed in the I/V characteristics obtained under constant illumination. In GaAs, carrier recombination occurs on the ns timescale,[32–34] and therefore the transient effect we observe here cannot be attributed to this phenomenon, as the decay time is in the ms regime. However, it could be due to hole trapping, since photo-generated holes can be trapped at surface states[35,36] with much longer lifetimes. Holes trapped in surface states will increase the positive charge at the surface and therefore reduce the band bending. Since reduced band bending means that the radius of the space charge region is smaller, hole trapping also reduces the area that contributes charge carriers to the photocurrent, so the photocurrent decreases until a steady state is reached (more details in the SI). As can be observed in Figure 4, the transient effect for **PDT** is more pronounced than for **1Ph1**. We attribute this to the presence of the frontier orbital of the molecular wire, which allows trapped holes to escape to the Au electrode, reducing the charge build-up. The energy level alignment is more efficient in the case of **1Ph1** than for **PDT**, resulting in the decreased transient effect of the former and its faster approach to the steady state value. As expected, transient effects become less strong with increasing chopping frequency, as less time is given for discharge after illumination is turned OFF, so the surface remains more positive. The effect is also observable only on $GaAs^{LD}$ because the space charge region is much larger than in $GaAs^{HD}$, so the effect of a change in band bending induced by holes accumulated at the surface on the volume in which the photocurrent is generated can be much larger.

PREPRINT

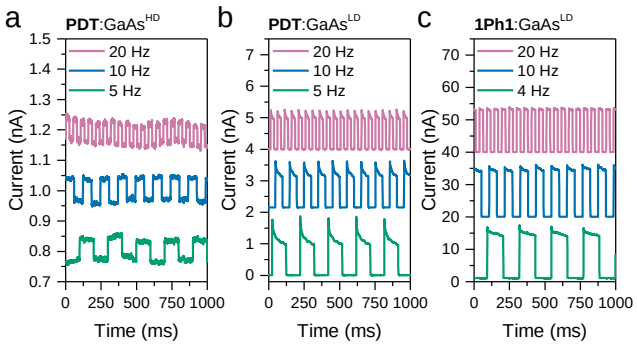

Figure 4: Photocurrent *vs* time traces for **PDT** on $GaAs^{HD}$ (a) and $GaAs^{LD}$ (b), and **1Ph1** on $GaAs^{LD}$ (c). Traces are obtained after engaging the tip in forward bias (-1.5 V), disabling the feedback loop, reversing the bias to +1.5 V and alternating the junction between dark and laser illumination conditions with a mechanical chopper. Traces are offset on the *y* axis for clarity. Dark current is 0.75 nA in (a), 3.8 pA in (b), and 21 pA in (c).

Having established the basic behavior of a MMS nanodevice, we then proceeded to the characterization of the contribution of a single molecule to the overall current transported. Data presented in the preceding sections is taken under conditions where the STM tip is interacting with an undefined (albeit small) number of molecules. To characterize single-molecule junctions we employed the "blinking" or "I(t)" approach,[27] where the current is monitored as a function of time with the feedback loop disabled, and we observe the stochastic formation and rupture of single-molecule bridges in the device. This process is described in detail in a previous publication[12] and briefly in the methods section. **PDT** on $GaAs^{LD}$ in forward bias resulted in frequent current jumps (Figure 5 (a)), albeit noisier than the results obtained on $GaAs^{HD}$.[12] We collected traces over a long period of time, showing such single-molecule events, that were subsequently sliced at the beginning and end of each current jump. The results were compiled in histograms and density maps to visualize the magnitude of the current jumps and the stability over time of the single-molecule junctions. In forward bias conditions (-1.5 V) this procedure gave data that could be compiled in a histogram with a clear peak at 1.05 nA, with stable junctions lasting longer than 500 ms (Figure 5 (b)).

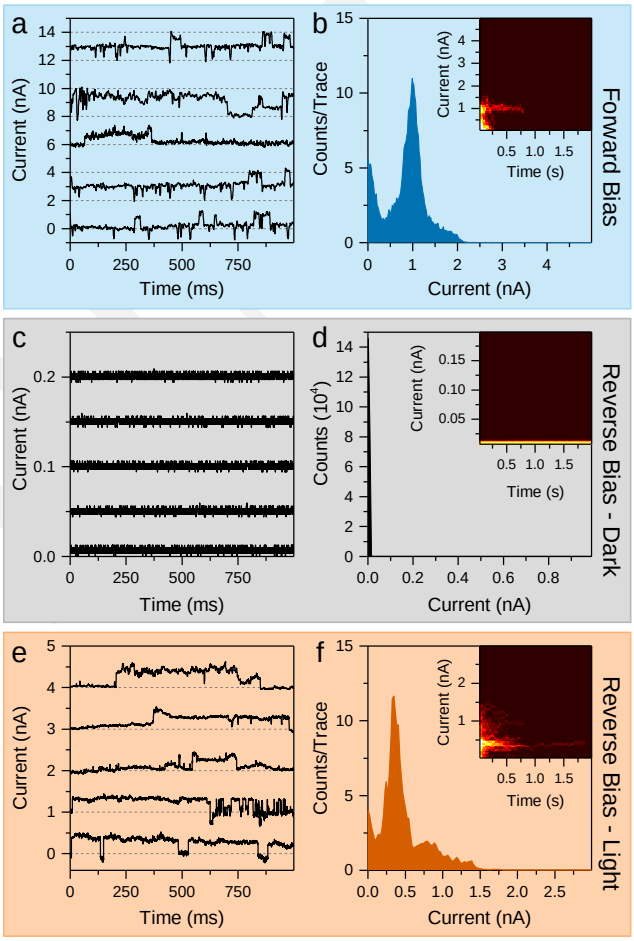

Figure 5: 1000 ms cutouts of current *vs* time traces in forward bias at -1.5 V (a), in reverse bias at +1.5 V in the dark (c) and under constant illumination (e) for **PDT**. Traces are recorded after engaging the tip in forward bias, with the feedback loop disabled, and are offset on the *y* axis for clarity. Histograms compiled from sliced traces in forward bias (b) and reverse bias in the dark (d) or under illumination (f), with relative density map (inset) showing the stability over time of a single-molecule junction. Histograms and inset density maps in (b) and (e) are compiled from, respectively, 744 and 705 slices. Histogram in (d) compiled from current recorded over 20 minutes, and sliced in 2 s portions to give the inset 2d map.

In the dark under reverse bias conditions (+1.5 V), no significant jumps could be detected in the current *vs* time traces (Figure 5 (c)), and the current flow through the device was very small (dark current of ~4 pA). However, when the junction was illuminated, sudden current jumps could be observed again over time. Compiling the current vs time traces in a statistical histogram resulted in a main peak at 0.38 nA, with junctions of similar temporal stability to those observed in the dark (Figure 5 (f)). The difference in magnitude of the current jumps under forward and reverse bias conditions is not surprising, because the current through the molecule depends on how much of the potential drop across the junction (the bias) is applied across the molecule and how much across the space charge zone of the semiconductor. There is no reason to assume that this distribution would be the same in forward and reverse bias, as it will be affected by factors such as the hole trapping previously discussed.

In conclusion, we demonstrate here a metal-molecule-semiconductor nanodevice, with Au and GaAs contacts, that acts as a photodiode. Using GaAs with lower doping density, we greatly reduce the dark current and increase the photocurrent in reverse bias. The choice of molecular wire tethering the metal and the semiconductor also plays an important role in the overall charge transport across the device upon illumination, with the energy gaps between the Fermi level and the frontier molecular orbitals being a major factor in determining the photocurrent magnitude. We propose a mechanism of charge transport for the illuminated reverse-biased junction, where photo-generated holes tunnel to the metal assisted by a molecular orbital (the HOMO). The non-planar geometry of the space charge layer results in a photocurrent that does not plateau like a planar junction, and also explains why decreasing the doping density gives such a large increase in photocurrent. Single-molecule transport was analysed statistically, with the main result being that molecular contributions to the overall current across the reverse-biased junction could only be observed under illumination. In reverse bias conditions, the absence of current jumps in the absence of illumination and the very low dark current value provided by $GaAs^{LD}$. ensures that only photo-generated charge carriers can be transported across the junction. As the charge carriers could be spin-polarized by illuminating GaAs with circularly polarized light, our work paves the way to single-molecule photospintronics.

Methods

Chemicals: **PDT**, GaIn eutectic and NH_4OH 30% aqueous solution were purchased from Sigma-Aldrich. **1Ph1** was purchased from TCI UK. Solvents and HCl 37 % were purchased from Thermo Fisher Scientific. All chemicals were used without further purification.

Sample Preparation: In a typical experiment, an ohmic contact (GaIn eutectic) is painted with a small brush on the back of the GaAs slide ($GaAs^{HD}$: Si-doped, n-type, <100> ± 0.05º, carrier concentration 3 × 10^{18} cm^{-3}; $GaAs^{LD}$: Si-doped, n-type, <100> ± 0.03º, carrier concentration 1.5-1.7 × 10^{17} cm^{-3}; both from Wafer Technology Ltd.) and then annealed at 400 ºC in vacuum (~ 10^{-5} bar) for 90 minutes. The wafer is then chemically etched in concentrated ammonia to remove the native oxides for 5 minutes, rinsed with ultrapure Type 1 water and absolute ethanol, and

immediately immersed in a degassed ethanol solution containing 1 mM of the desired molecular wire and 5 % concentrated ammonia solution (to avoid oxide layer regrowth). Samples were incubated under Ar atmosphere for 24 hours, removed from solution, copiously rinsed with ethanol, dried under a stream of Ar, and placed on a Au substrate (gold-on-glass, Arrandee), with an additional layer of fresh GaIn eutectic painted to provide optimal contact (schematics of device structure in Figure 1).

STM Measurements: An STM (Keysight Technology 5500 SPM) equipped with an electrochemically etched Au tip (ethanol:HCl 37 %, 1:1, 2.5 V) was used to fabricate and characterize the MMS devices presented in this study. The sample was mounted on the STM stage and the gold tip was advanced towards the substrate in forward bias (substrate at -1.5 V relative to the tip) conditions by increasing the setpoint current until sudden jumps were observed in the current signal. These jumps have been related to a change in charge transport from tunneling through air to tunneling through the molecular backbone.[17,37–39] Once the tip was in contact with the monolayer, we recorded *I / V* characteristics by sweeping the bias between -1.5 and +1.5 V at 3 V/s, both in the dark and under laser (Toshiba LHG-3220 3 mW He-Ne tube, 632.8 nm) illumination. We employed a linear preamp (10 nA/V) for the characterization of junctions with molecular bridges, and a logarithmic preamp for the Au:GaAs^{LD} "hard contact". Data presented in the manuscript is the average of 25 curves, obtained from different positions on the substrates. Single-molecule junction formation/rupture events could be observed in individual *I / V* characteristics, and examples of such events can be found in the SI. The feedback loop was then disabled with the tip engaged, the bias reversed to +1.5 V, and current *vs* time traces were recorded while interrupting the laser beam with a rotating disc optical chopper (Bentham Instruments 218 variable frequency optical chopper). To minimize the effect of junction formation/rupture, we recorded this data at a slightly (100-200 pA) higher setpoint, with the tip therefore more embedded in the molecular monolayer. Examples of traces showing single-molecule events during the recording of such traces are presented in the SI. After recording each trace, we returned to forward bias, and the feedback loop was re-engaged to minimize drift. For single-molecule transport studies, the tip was re-engaged to the monolayer in forward bias at the lowest setpoint that yielded current jumps. With the feedback loop disabled, we recorded current traces in forward bias, before reversing the bias to record the corresponding current traces in dark conditions and under illumination. Current jumps were monitored this way over several hours, and processed using software written in Python which has been described previously.[12] In brief, the background setpoint current was automatically determined and then subtracted from the raw current *vs.* time traces. Individual traces were then sliced into segments by locating jumps between the different current levels using features in the differential of the current (*dI / dt*). These slices were afterwards compiled into current histograms and current *vs* time density plots.

Associated Content

Space charge layer thickness calculations and further STM studies. The material is available free of charge

PREPRINT

on the ACS Publications website. Raw data is available in the catalog in Liverpool at: https://datacat.liverpool.ac.uk/id/eprint/345 or at DOI: 10.17638/datacat.liverpool.ac.uk/345.

Author Information

Corresponding Authors

*E-mail: nichols@liv.ac.uk
w.schwarzacher@bristol.ac.uk

Notes

The authors declare no competing financial interest.

Acknowledgements

We thank EPSRC for funding, under grants EP/M005046/1 (Liverpool) and EP/M00497X/1 (Bristol).

Bibliography

(1) Reed, M. A.; Zhou, C.; Muller, C. J.; Burgin, T. P.; Tour, J. M. *Science* **1997**, *278* (5336), 252–254.

(2) Xu, B.; Tao, N. *Science* **2003**, *301* (5637), 1221–1223.

(3) Haiss, W.; van Zalinge, H.; Higgins, S. J.; Bethell, D.; Höbenreich, H.; Schiffrin, D. J.; Nichols, R. J. *J. Am. Chem. Soc.* **2003**, *125* (50), 15294–15295.

(4) Xiang, D.; Jeong, H.; Kim, D.; Lee, T.; Cheng, Y.; Wang, Q.; Mayer, D. *Nano Lett.* **2013**, *13* (6), 2809–2813.

(5) Ko, C. H.; Huang, M. J.; Fu, M. D.; Chen, C. H. *J. Am. Chem. Soc.* **2010**, *132* (2), 756–764.

(6) Peng, Z. L.; Chen, Z. Bin; Zhou, X. Y.; Sun, Y. Y.; Liang, J. H.; Niu, Z. J.; Zhou, X. S.; Mao, B. W. *J. Phys. Chem. C* **2012**, *116* (41), 21699–21705.

(7) Park, Y. S.; Whalley, A. C.; Kamenetska, M.; Steigerwald, M. L.; Hybertsen, M. S.; Nuckolls, C.; Venkataraman, L. *J. Am. Chem. Soc.* **2007**, *129* (51), 15768–15769.

(8) Moreno-García, P.; Gulcur, M.; Manrique, D. Z.; Pope, T.; Hong, W.; Kaliginedi, V.; Huang, C.; Batsanov, A. S.; Bryce, M. R.; Lambert, C.; Wandlowski, T. *J. Am. Chem. Soc.* **2013**, *135* (33), 12228–12240.

(9) Leary, E.; La Rosa, A.; González, M. T.; Rubio-Bollinger, G.; Agraït, N.; Martín, N. *Chem. Soc. Rev.* **2015**, *44* (4), 920–942.

(10) Reuter, M. G.; Hansen, T.; Seideman, T.; Ratner, M. A. *J. Phys. Chem. A* **2009**, *113* (16), 4665–4676.

(11) Rakshit, T.; Liang, G. C.; Ghosh, A. W.; Datta, S. *Nano Lett.* **2004**, *4* (10), 1803–1807.

(12) Vezzoli, A.; Brooke, R. J.; Ferri, N.; Higgins, S. J.; Schwarzacher, W.; Nichols, R. J. *Nano Lett.* **2017**, *17* (2), 1109–1115.

(13) Prins, F.; Barreiro, A.; Ruitenberg, J. W.; Seldenthuis, J. S.; Aliaga-Alcalde, N.; Vandersypen, L. M. K.; van der Zant, H. S. J.

PREPRINT

Nano Lett. **2011**, *11* (11), 4607–4611.

(14) Kim, T.; Liu, Z.-F.; Lee, C.; Neaton, J. B.; Venkataraman, L. *Proc. Natl. Acad. Sci.* **2014**, *111* (30), 10928–10932.

(15) Guo, X.; Small, J. P.; Klare, J. E.; Wang, Y.; Purewal, M. S.; Tam, I. W.; Hong, B. H.; Caldwell, R.; Huang, L.; O'Brien, S.; Yan, J.; Breslow, R.; Wind, S. J.; Hone, J.; Kim, P.; Nuckolls, C. *Science* **2006**, *311* (5759), 356–359.

(16) Jia, C.; Migliore, A.; Xin, N.; Huang, S.; Wang, J.; Yang, Q.; Wang, S.; Chen, H.; Wang, D.; Feng, B.; Liu, Z.; Zhang, G.; Qu, D.-H.; Tian, H.; Ratner, M. A.; Xu, H. Q.; Nitzan, A.; Guo, X. *Science* **2016**, *352* (6292), 1443–1445.

(17) Aragonès, A. C.; Darwish, N.; Ciampi, S.; Sanz, F.; Gooding, J. J.; Díez-Pérez, I. *Nat. Commun.* **2017**, *8*, 15056.

(18) Guisinger, N. P.; Yoder, N. L.; Hersam, M. C. *Proc. Natl. Acad. Sci.* **2005**, *102* (25), 8838–8843.

(19) Lodha, S.; Carpenter, P.; Janes, D. B. *J. Appl. Phys.* **2006**, *99* (2), 24510.

(20) McGuiness, C. L.; Shaporenko, A.; Mars, C. K.; Uppili, S.; Zharnikov, M.; Allara, D. L. *J. Am. Chem. Soc.* **2006**, *128* (1), 5231–5243.

(21) Budz, H. A.; Biesinger, M. C.; LaPierre, R. R. *J. Vac. Sci. Technol. B Microelectron. Nanom. Struct.* **2009**, *27* (2), 637.

(22) Darwish, N.; Aragonès, A. C.; Darwish, T.; Ciampi, S.; Díez-Pérez, I. *Nano Lett.* **2014**, *14* (12), 7064–7070.

(23) Martin, S.; Haiss, W.; Higgins, S. J.; Nichols, R. J. *Nano Lett.* **2010**, *10* (6), 2019–2023.

(24) Tam, E. S.; Parks, J. J.; Shum, W. W.; Zhong, Y.; Santiago-Berríos, M. B.; Zheng, X.; Yang, W.; Chan, G. K.-L.; Abruña, H. D.; Ralph, D. C. *ACS Nano* **2011**, *5* (6), 5115–5123.

(25) Dulić, D.; van der Molen, S.; Kudernac, T.; Jonkman, H.; de Jong, J.; Bowden, T.; van Esch, J.; Feringa, B.; van Wees, B. *Phys. Rev. Lett.* **2003**, *91* (20), 207402.

(26) Battacharyya, S.; Kibel, A.; Kodis, G.; Liddell, P. a; Gervaldo, M.; Gust, D.; Lindsay, S. *Nano Lett.* **2011**, *11* (7), 2709–2714.

(27) Haiss, W.; Nichols, R. J.; van Zalinge, H.; Higgins, S. J.; Bethell, D.; Schiffrin, D. J. *Phys. Chem. Chem. Phys.* **2004**, *6*, 4330–4337.

(28) Eckhardt, C.; Madl, M.; Brezna, W.; Smoliner, J. *J. Appl. Phys.* **2011**, *109* (3).

(29) Farsinezhad, S.; Sharma, H.; Shankar, K. *Phys. Chem. Chem. Phys.* **2015**, *17* (44), 29723–29733.

(30) Li, C.; Pobelov, I.; Wandlowski, T.; Bagrets, A.; Arnold, A.; Evers, F. *J. Am. Chem. Soc.* **2008**, *130* (1), 318–326.

(31) Brooke, C.; Vezzoli, A.; Higgins, S. J.; Zotti, L.

PREPRINT

A.; Palacios, J. J.; Nichols, R. J. *Phys. Rev. B* **2015**, *91* (19), 195438.

(32) Rastegar, B.; Wager, J. F. *Semicond. Sci. Technol.* **1986**, *1* (3), 207.

(33) Arakawa, Y.; Sakaki, H.; Nishioka, M.; Yoshino, J.; Kamiya, T. *Appl. Phys. Lett.* **1985**, *46* (5), 519–521.

(34) De Dios-Leyva, M.; Oliveira, L. E. *J. Appl. Phys.* **1994**, *75* (1), 660–662.

(35) Kelly, J. J. *J. Electrochem. Soc.* **1983**, *130* (12), 2452.

(36) Hoffmann, P. M.; Oskam, G.; Searson, P. C. *J. App. Phys.* **1998**, *83* (8), 4309.

(37) Haiss, W.; Wang, C.; Grace, I.; Batsanov, A. S.; Schiffrin, D. J.; Higgins, S. J.; Bryce, M. R.; Lambert, C. J.; Nichols, R. J. *Nat. Mater.* **2006**, *5* (12), 995–1002.

(38) Huang, S.; He, J.; Chang, S.; Zhang, P.; Liang, F.; Li, S.; Tuchband, M.; Fuhrmann, A.; Ros, R.; Lindsay, S. *Nat. Nanotechnol.* **2010**, *5* (12), 868–873.

(39) Chang, S.; He, J.; Kibel, A.; Lee, M.; Sankey, O.; Zhang, P.; Lindsay, S. *Nat. Nanotechnol.* **2009**, *4* (5), 297–301.

PREPRINT